Colloid Polym Sci 274:368–374 (1996)

ORIGINAL CONTRIBUTION

T. Okubo
H. Fujita

Phase diagram of alloy crystal in the exhaustively deionized suspensions of binary mixtures of colloidal spheres

Received: 25 July 1995
Accepted: 13 September 1995

Prof. Dr. T. Okubo[1] (✉) · H. Fujita
Department of Polymer Chemistry
Faculty of Engineering
Kyoto University
Kyoto 606-01, Japan

[1] *Current address*:
Department of Applied Chemistry
Faculty of Engineering, Gifu University
Gifu 501-11, Japan

Abstract Phase diagrams of liquid-like, alloy crystal-like and amorphous solid-like(AS) structures have been obtained for the exhaustively deionized aqueous suspensions of the binary mixtures of polystyrene or silica spheres. Diameter, polydispersity index (standard deviation of diameter divided by the mean diameter) and size ratio of the binary spheres (diameter of small sphere divided by that of large one) range from 85 to 136 nm, 0.07 to 0.26 and 0.76 to 0.93, respectively. Close-up color photographs of the alloy crystals are taken and the crystal structure has been analysed from reflection spectroscopy. Most of the alloy crystals are *substitutional solid-solution* (sss) type and body-centered cubic lattice structure. Formation of the alloy crystals is attributed to the important role of the expanded electrical double layers in the deionized condition and increase toward unity in the effective size ratio, which is the effective diameter of small sphere including double layer divided by that of large sphere. AS structure is formed at the rather high concentrations of two spheres, where the thickness of the electrical double layer is thin and the effective size ratio is comparatively small.

Key words Colloidal crystals – polystyrene spheres – silica spheres – alloy crystals – electrical double layer

Introduction

Colloidal crystals are very beautiful and fantastic, since the intersphere distance is just in the range of light wavelength and they reflect light by the Bragg reflection [1–12]. The mechanism of crystal growth and the morphology of colloidal single crystals are quite similar to those of typical crystals such as metals and protein crystals. The colloidal crystals are ideal systems for model studies of crystals, since the crystal structures are analyzed with the optical techniques and intersphere interaction are readily manipulated by controlling the composition of the suspension. Furthermore, phase transition phenomena such as crystallization and melting occur very sharply.

Generally speaking, crystal structures of monodispersed colloidal spheres are face-centered cubic (fcc) (or close-packing) or body-centered cubic (bcc) lattices in suspensions [13]. From many data, it may be concluded that the fcc lattices are most stable and they transform to the bcc lattice (a) at low sphere concentrations, (b) in the presence of salts, (c) at elevated suspension temperature, (d) for spheres of high charge densities, and (e) at high pressure. Coexistence of fcc and bcc structures has often been observed. The transformation between the subphases of fcc and bcc lattices is highly related to the change in the *dead space* regions, which particles do not occupy. The fcc structure gives less dead space compared with the bcc form, for example. Note that the ordered distribution of anisotropic shaped particles in suspension is determined

exclusively by the condition of the *minimum dead space* [14–16]. Amorphous solid-like (glass-like) structures have been also formed mainly under the influence of the principle of the minimum dead space [17].

Alloy structures are formed in colloidal suspensions of binary mixtures of spheres of different sizes. The superlattice structures observed in colloidal systems mainly by Hachisu et al. are AlB_2, $NaZn_{13}$, $CaCu_5$, $MgCu_2$, NaCl and AB_4 types [18–24]. Note that these alloy structures are mainly determined by the principle of the minimum dead space and then by the changes in the effective size ratio, i.e., effective size of small spheres containing the electrical double layer thickness against that of large spheres [20, 25], and the segregation effect [26]. Recently, crystallization of binary mixtures of spheres of diameter ratios (including no double layers) of 0.58 and 0.62 have been discussed in detail [27, 28]. The amorphous solid-like structures have been formed in binary mixtures of large and small spheres [10, 29, 30].

The region where small ions distribute is called as the *electrical double layer*. Thickness of the electrical double layers is approximated by the Debye-screening length, l_{DH} given by Eq. (1).

$$l_{DH} = (4\pi e^2 n/\varepsilon k_B T)^{-1/2}, \quad (1)$$

where, e is the electronic charge, and ε is the dielectric constant of the solvent. n is the concentration of "*diffusible*" or "*free-state*" cations and anions in suspension. Thus, n is the sum of the concentrations of diffusible counterions, foreign salt and both H^+ and OH^- from the dissociation of water. Maximum value of l_{DH} in water is ca. 1 μm, which is estimated from Eqs. (1) by taking $n = 2 \times 10^{-7}\,(\text{mol/dm}^3) \times N_A \times 10^{-3}\,\text{cm}^{-3}$, where N_A is Avogadro's number. Formation of the crystal-like ordering is explained nicely with the *effective hard-sphere model* [31–35].

Recently, we have observed very large single crystals, 2 to 8 mm in size for the very *diluted* aqueous suspension (ca. 0.0002 in volume fraction) and also exhaustively *deionized* suspension with ion-exchange resins more than three weeks in a test tube of 13 mm in outside diameter [36–39]. In this report, the phase diagram is obtained for the binary mixtures of spheres in the *exhaustively deionized suspensions* with the ion-exchange resins for three to four weeks.

Experimental

Materials

Colloidal silica spheres of CS-81 and CS-121 were gift from Catalyst & Chemicals Ind. Co. (Tokyo). D1C25, D1C27, D1B76, D1P30 and D1K88 were polystyrene spheres purchased from Dow Chemical Co. Diameter (d), standard deviation (δ) from the mean diameter, and polydispersity index (δ/d) are listed in Table 1. The values of d and δ were determined from an electron microscope. The charge densities of the strongly acidic groups of spheres, which are originated mainly from the silanol groups at the sphere surfaces, were determined by conductometric titration with a Wayne–Kerr autobalance precision bridge, model B331, mark II (Bogner Regis, Sussex) or a Horiba conductivity meter, model DS-14 (Kyoto). All these spheres were carefully purified several times using an ultrafiltration cell (model 202, membrane: Diaflo-XM300, Amicon Co.). Then the samples were treated on a mixed bed of cation- and anion-exchange resins [Bio-Rad, AG501-X8(D), 20–50 mesh] for at least 1 month. Water used for the purification and for suspension preparation was deionized by using cation- and anion-exchange resins [Puric-R, type G10, Organo Co. (Tokyo)] and further purified by a Milli-Q reagent grade system (Millipore Co., Bedford, MA). Colloidal suspension was prepared by pouring two deionized stock suspensions and the deionized water with the resins into a disposable culture tube (borosilicate glass, Corning Glass Works, Corning, N.Y., 11 and 13 mm, inside and outside diameters) shielded tightly several ten layers with Parafilm (American Can Co., Greenwich, CT). The sample suspensions were treated with a small amount of Bio-Rad resins more than 3 weeks with up-and-down mixing several times a day.

Close-up photographing

Phase equilibria between the crystal-like and liquid-like structures were observed clearly with the naked eyes. Close-up photographing of colloidal crystals in a test tube was made with a Canon EOS10 camera, macro-lens (EF50 mm, $f = 2.5$) and life-size converter EF. Velvia film(Fujichrome, RVP135, ISO = 50) was used. Light source was a pocket-type flash light (Xenon type, BF-775, National).

Table 1 Properties of spheres used

Sphere	d (nm)	δ (nm)	δ/d	Charge density (μC/cm^2) strong acid	weak acid
CS-81	103	13.2	0.13	0.38	–
CS-121	136	10.9	0.08	0.40	–
D1C25	85	6	0.07	1.5	1.0
D1C27	91	6	0.066	2.0	1.4
D1B76	109	3	0.0028	2.1	0.71
D1P30	109	27.8	0.26	0.62	0.32

Reflection-spectrum measurements

The reflection spectra at an incident angle of 90° were recorded on a multichannel photodetector, MCPD-110B, Otsuka Electronics, Hirakata, Osaka, connected to a *Y*-type optical-fiber cable.

Results and discussion

CS121 and CS81 mixtures

First, we discuss the crystal formation for the binary mixtures of CS121 and CS81 spheres at 0.76 in the size ratio, γ ($= d_B/d_A$, where d_A and d_B are the diameters of large and small spheres in the mixture). The width for the picture of Fig. 1 corresponds to the outer diameter of the observation cell, 13 mm. Very large and beautiful single crystals have been observed at rather low sphere concentrations ($\phi_A = 0.000435$, $\phi_B = 0.000575$) and in the exhaustively deionized suspension. The suspensions exhibiting brilliant single crystals were rather transparent. In this picture a background is dark, but the suspension must be full of single crystals surrounded with grain boundaries. With a slow rotation of the cell, bright patterns of single crystals changed rapidly. Change in colors from bluish to reddish is due to the change in the incident angles of light through the curved wall of the test tube. Crystal planes are recognized for some crystals clearly. Two kinds of single crystals, i.e., block-like ones in the bulkphase far from the cell wall and pillar-like ones along the cell wall, are observed. These are formed from the homogeneous- and heterogeneous-nucleation mechanisms. These features of the alloy single crystals are quite similar to those observed for the aqueous suspension of single kind of spheres [36–38].

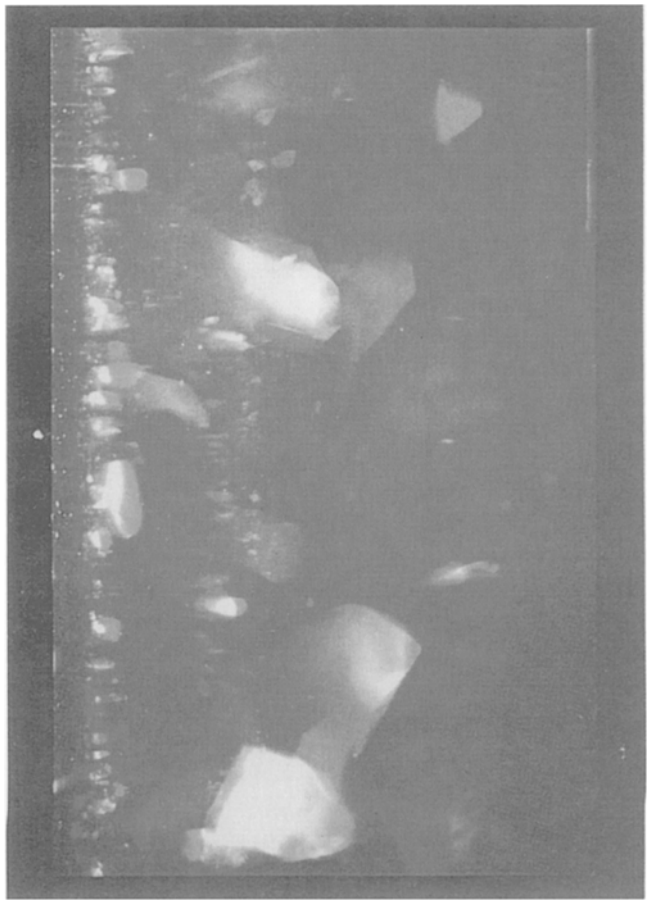

Fig. 1 A close-up color picture of CS121 ($\phi = 0.000435$) + CS81 ($\phi = 0.000575$) mixture 20 min after inverted mixing the suspension which has been treated with Bio-Rad resins for 4 weeks in the cell. Exposure = 2 s, iris = 22

Figures 2(a) and 2(b) show the phase diagram of CS121 and CS81 mixtures in the low and high ranges of ϕ_A and/or ϕ_B, respectively. The open and solid circles in Fig. 2(a) are the *crystal-like* and *liquid-like* structures, respectively. Five different sizes of open circles in the figures indicate the round size of the single crystals which appeared, i.e., smaller than 0.1 mm (shown by the smallest open circles in the figures), 0.1 to 0.5 mm (secondary small open circles), 0.5 to 1.5 mm (medium size in Fig. 2(b)), 1.5 to 2.5 mm (secondary large open circles) and larger than 2.5 mm (largest open circles in Fig. 2(b)), respectively. Figure 2(a) shows that the critical concentrations of melting for this binary system, $\phi_{A,c}$ and $\phi_{B,c}$ are also quite low. However, these values were larger than the mean values of $\phi^0_{A,c}$ and $\phi^0_{B,c}$, which are the critical concentrations of melting for the suspensions of single kind of spheres and locate just on the line connecting $\phi^0_{A,c}$ in the X-axis and $\phi^0_{B,c}$ in the Y-axis of Fig. 2(a). As was described above, the very large single crystals are formed at the low sphere concentrations in the binary mixture, lower than 0.001 in volume fraction as is seen in Fig. 2(a).

Here, let us discuss the effective size ratio, γ_{eff} including the electrical double layers, which coat the spheres and move simultaneously with the spheres. γ_{eff} is given by Eq. (2).

$$\gamma_{eff} = d_{B,eff}/d_{A,eff} = (d_B + 2 \times l_{DH})/(d_A + 2 \times l_{DH}) \,. \qquad (2)$$

The n-value in Eq. (1) is the sum of the concentrations of diffusible (or free state) counterions (n_c), foreign salt (n_s) and both H^+ and OH^- from the dissociation of water (n_0). In the deionized suspension, n_s is zero and then n is

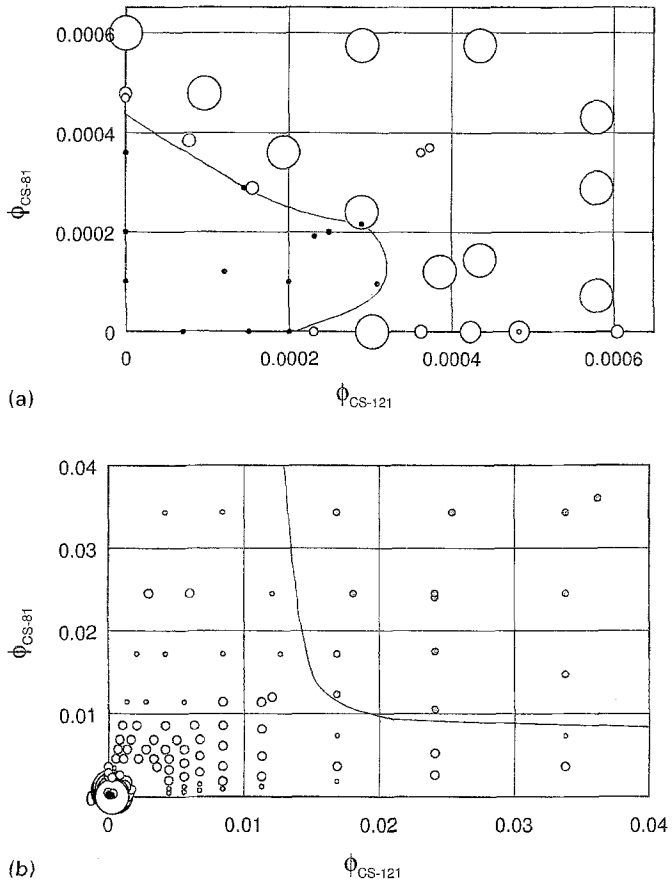

Fig. 2A Phase diagram of CS121+CS81 mixtures at 23 °C. Open and solid circles show the "crystal" and "liquid" phases, respectively; **B** Phase diagram of CS121+CS81 mixtures at 23 °C. Open and dotted circles show the "crystal" and "amorphous solid" phases, respectively

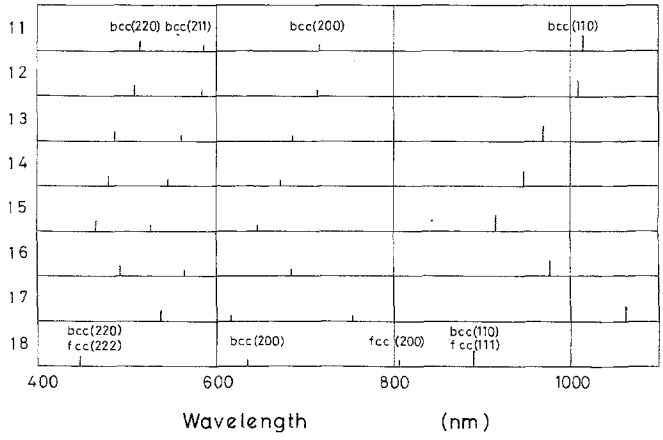

Fig. 3 Peak wavelengths in the reflection spectra of CS121+CS81 mixtures at 23 °C. Codes 11: $\phi_A = 0.000846$, $\phi_B = 0.00686$, 12: 0.00169, 0.00686, 13: 0.00338, 0.00686, 14: 0.00508, 0.00686, 15: 0.00676, 0.00686, 16: 0.00676, 0.00490, 17: 0.00676, 0.00294, 18: 0.00423, 0.00858

given by Eq. (4).

$$n = n_c + n_s + n_0 \tag{3}$$

$$n = \{2 \times 10^{-7} + (Q_A \beta_A \phi_A / 1.606\, d_A) + (Q_B \beta_B \phi_B / 1.606\, d_B)\} \times N_A \times 10^{-3}\,. \tag{4}$$

Here, Q_A and Q_B are the surface charge densities of strongly acidic groups of spheres, A and B. β_A and β_B are the fraction of *free state* counterions. The β-values of all the spheres used in this work were estimated to be 0.1 [2, 40–42]. Using Eq. (4), l_{DH} and γ_{eff} were estimated to be 885 nm and 0.98 at $\phi_A = \phi_B = 0.0003$. This value of γ_{eff} in the range of sphere concentrations bit higher than the critical concentration of melting in Fig. 2(a), is very close to unity, and this means that the difference in the effective diameters of large and small spheres is quite small, ca. 2%. Clearly, the apparent high monodispersity in the effective diameters is essential for the formation of giant single crystal at low sphere concentrations in the binary system. Crystal structure of the alloy crystals is now easily deduced to be *substitutional solid solution* (s.s.s.)-type (or mixed crystals), since the effective diameter of two spheres are very close to each other *within two percent.*

The peak wavelengths in the reflection spectra of several alloy crystals are compiled in Fig. 3. Length of the bars in the figure shows the sharpness and strength of the intensity of the reflection peaks very roughly. Most peaks have belonged to the (110), (200), (211) and (220) planes of bcc lattice structure as is shown in the figure. However, mixture of the bcc and fcc lattices were sometimes and fcc only were seldom observed. Scattering vectors at the observed peaks, which are calculated using the peak wavelength, agreed with the calculated ones from the second form of Miller indices excellently.

In order to check validity of the effective hard-sphere model for the binary systems, the effective mean diameter, $d_{m,eff}$ in Eq. (5) was compared with the mean intersphere distance, l_m given in Eq. (6) in the alloy crystal at the border of the transition between liquid and crystal in Fig. 4.

$$d_{m,eff} = d_A x + d_B(1 - x) + 2l_{DH} \tag{5}$$

$$l_m = [\phi_A / 0.68\, d_A^3 + \phi_B / 0.68\, d_B^3]^{-1/3}\,, \tag{6}$$

where x is the fraction of large sphere concentration given by $\phi_A/(\phi_A + \phi_B)$. For the deionized suspensions of single spheres, the validity of the effective hard-sphere model has been supported strongly [38]. It is clear in the figure that the relation of $d_{m,eff} \geq l_m$ holds also for the binary systems.

The dotted circles in the high sphere concentrations in Fig. 2(b) indicate the amorphous solid-like (AS)

distribution, which was recognized with the naked eyes from the faint iridescent color. Figure 5 shows the changes in the reflection spectra in the region of phase transition between crystal-like and AS structures. Reflection peaks of the crystal-like suspensions from curves 1 to 4 and 7 to 8 were not very sharp, since crystals was small for these conditions. However, reflection peaks corresponding to the AS structures were quite broad and their intensities were also very weak. It should be noted in Fig. 5 that the intensities of the reflection light from the AS structure were highly amplified compared with the peaks attributed to the crystal. The peak profile of the AS structure is very similar to that of liquid-like distribution. AS structures have been often observed for the deionized suspensions of highly polydispersed particles hitherto [43, 44]. It should be noted here that the radial distribution function, $g(r)$ of the amorphous solid-like distribution resembles the liquid-like patterns, the broad peak appears for the two structures. However, the difference between them is quite distinct; particles in the liquid-like distribution move vigorously and comparatively freely, but the distances between adjacent particles are similar. On the other hand, particles in the amorphous solid-like structure does not move far and move only vibrationally around their equilibrium points. It should be mentioned here that shift in the peak wavelengths in Fig. 5 is nicely explained with Eq. (6). The values of l_{DH} and γ_{eff} at $\phi_A = \phi_B = 0.017$ in the phase of amorphous structure but close to the region of the crystal-like distribution was evaluated to be 292 nm and 0.95 by using Eq. (2). Thus, it may be concluded that the AS structure is formed when γ_{eff} is smaller than 0.95. When γ_{eff} is between 0.95 and 0.98, crystal-like structure are formed.

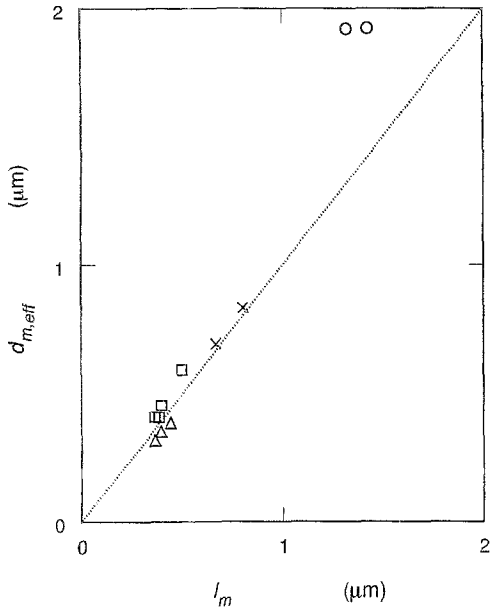

Fig. 4 Comparison of $d_{m,eff}$ and l_m. ○: CS121 + CS81, X: D1C27 + D1C25, Δ: D1B76 + D1C25, □: D1P30 + D1C25

D1C27 and D1C25 mixtures

The true size ratio, γ of D1C27 and D1C25 mixture is 0.93, close to unity compared with the preceding system of CS121 and CS81. However, both D1C25 and D1C27 spheres are small in sphere size and high in monodispersity. Figure 6 shows the phase diagram of D1C27 and D1C25 mixtures. Open and solid circles indicate the crystal-like and liquid-like distributions, respectively. At a glance, the diagram is quite similar to that of CS121 and CS81 mixtures shown in Fig. 2(a), though the critical concentration for the suspension of D1C25, $\phi^0_{B,c}$ is much high (ca. 0.0014). As has been reported previously [38], the large critical concentration is due to the fact that the D1C25 spheres are not *definitely* large enough compared with the hydronium ions which form the electrical double layers, and the thermal movement of spheres are too vigorous to form the stable double layers around the spheres.

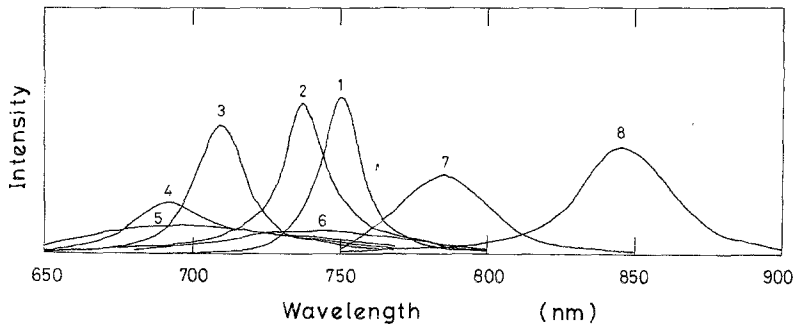

Fig. 5 Reflection spectra of CS121 + CS81 mixtures at 23 °C. Curves 1: $\phi_A = 0.00212$, $\phi_B = 0.0172$, 2: 0.00423, 0.0172, 3: 0.00845, 0.0172, 4: 0.0127, 0.0172, 5: 0.0169, 0.0172, 6: 0.0169, 0.0123, 7: 0.0169, 0.00735, 8: 0.0169, 0.00367

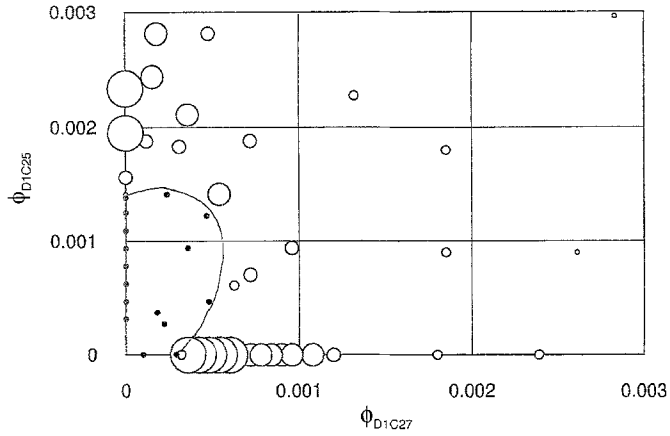

Fig. 6 Phase diagram of D1C27 + D1C25 mixtures at 23 °C. Open and solid circles show the "crystal" and "liquid" states, respectively

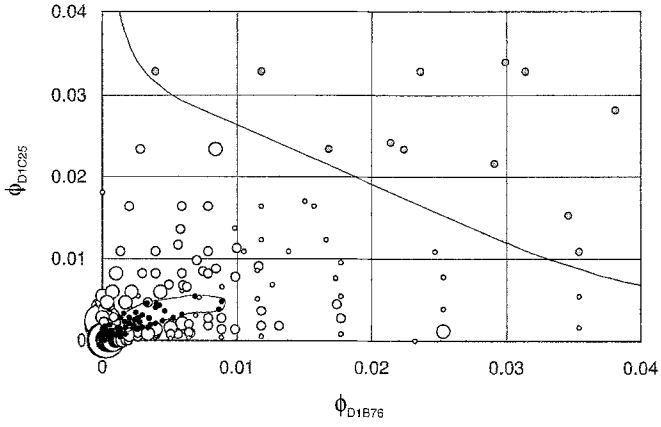

Fig. 7 Phase diagram of D1B76 + D1C25 mixtures at 23 °C. Open, solid and dotted circles show the "crystal", "liquid" and "amorphous solid" phases, respectively

From the analysis of the reflection spectra crystal structure of most of the alloy crystals were sss-type and bcc, though the graph demonstrating this was omitted in this paper. The effective size ratio, γ_{eff} at $\phi_A = \phi_B = 0.001$ were calculated as 0.99 (l_{DH} value was 262 nm). It is interesting to note that the similar value of γ_{eff} to CS121 + CS81 system was obtained.

D1B76 and D1C25 mixtures

True size ratio, γ is 0.78 for D1B76 and D1C25 mixtures. It is interesting to note that most of the single crystals look like the associates of small blocks (association-type), though a picture showing this was omitted here. The lozenge-shaped (rhombic) crystals, though they are not so perfect in shape, were also observed. These features are quite similar to those of D1C25 suspensions [38]. Figure 7 is the phase diagram of D1B76 and D1C25 mixtures. Open-, solid- and dotted-circles indicate the crystal-like, liquid-like and amorphous solid-like structures, respectively. Several characteristic features have been observed. First, size of the single crystals were not so large. Medium size was the largest among the crystals. Secondly, crystallization was disturbed effectively when large spheres were added into the suspension of small spheres. The critical concentration of melting of the suspension of the single component of spheres, D1B76, $\phi^0_{A,c}$ was 0.00016, whereas the critical concentration, $\phi_{A,c}$ of the mixture was ca. 0.008 in the largest case, ca. 50-fold large. On the other hand, the disturbing effect of small spheres of D1C25 was not so significant, i.e., $\phi^0_{B,c} = 0.0014$ and the largest value of $\phi_{B,c}$ was 0.0055. So, the ratio is ca. 4-fold only.

Effective size ratios at the several points at the crystal phases close to the critical curve of melting were calculated

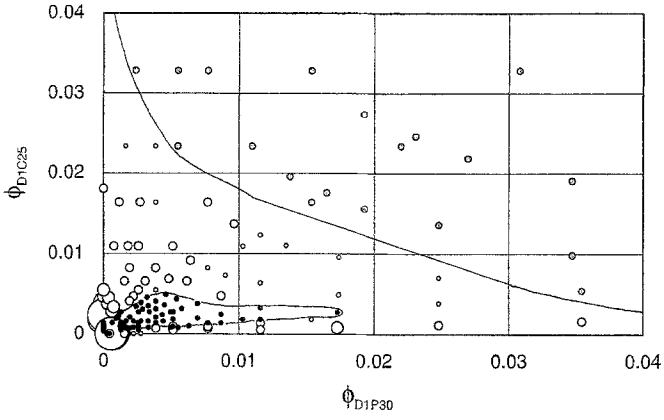

Fig. 8 Phase diagram of D1P30 + D1C25 mixtures at 23 °C. Open, solid and dotted circles show the "crystal", "liquid" and "amorphous solid" phases, respectively

using Eq. (4) to be 0.93, 0.92 and 0.94 at $\phi_A = \phi_B = 0.005$, $\phi_A = 0.01$; $\phi_B = 0.005$, and $\phi_A = 0.005$; $\phi_B = 0.0025$, respectively. Thus, the mean value of the effective size ratio is 0.93. Furthermore, the effective size ratios at the crystal-AS transition points were calculated as 0.90, 0.90 and 0.90, at $\phi_A = 0.01$; $\phi_B = 0.025$, $\phi_A = \phi_B = 0.02$ and $\phi_A = 0.03$; $\phi_B = 0.01$, respectively. The crystal phase is observed in the narrow range, $0.90 \leq \gamma_{eff} \leq 0.93$, and the amorphous solid phase is formed when γ_{eff} is smaller than 0.90. Lattice structure of the alloy crystals formed in the D1B76 + D1C25 mixtures has been assigned to be bcc from the reflection peak analyses. Furthermore, it is highly plausible that some super lattices such as $MgCu_2$ and $CaCu_5$ types are formed in the narrow region among the AS phase as was reported in a previous paper [24], though such lattices were not detected in this work.

D1P30 and D1C25 mixtures

Among the spheres used in this work polydispersity of D1P30 is quite large, $\delta/d = 0.26$ (see Table 1). Surprisingly, alloy crystals of sss-type were formed for the binary mixtures containing D1P30 spheres. As is clear in Fig. 8, phase diagram of D1P30 and D1C25 mixture is also similar to that of D1B76 + D1C25, though the area of the liquid sub-phase for the former is more expanded compared with that of the latter. Furthermore, crystal region of the former was more narrow than the latter, since the border region of the crystal and amorphous solid subphases shifted toward the lower concentrations of both spheres. The γ_{eff} value at the crystal phase close to the liquid were evaluated to be 0.94 and 0.94 at $\phi_A = \phi_B = 0.005$ and $\phi_A = 0.018$; $\phi_B = 0.0025$, respectively. Furthermore, γ_{eff} values at the border of crystal and amorphous solid were 0.92, 0.92 and 0.91 at $\phi_A = 0.02$; $\phi_B = 0.13$, $\phi_A = \phi_B = 0.015$ and $\phi_A = 0.005$; $\phi_B = 0.025$, respectively. Thus, crystal and amorphous solid subphases are formed in the ranges $0.92 \leq \gamma_{eff} \leq 0.94$ and $\gamma_{eff} < 0.92$, respectively. It is interesting to note that the alloy single crystals are formed also in the narrow region of γ_{eff}, from 0.92 to 0.94. Crystal lattice structure of the D1P30 + D1C25 mixture was mainly bcc lattice, and sometimes bcc + fcc mixtures.

Acknowledgment This work was supported by the Research Foundation for Opto-Science and Technology.

References

1. Luck W, Klier M, Wesslau H (1963) Ber Bunsenges Phys Chem 67:75, 84
2. Vanderhoff W, van de Hul HJ, Tausk RJM, Overbeek JThG (1970) In: Goldfinger (ed) Clean Surfaces: Their Prearation and Characterization for Interfacial Studies. Dekker, New York
3. Hiltner PA, Papir YS, Krieger IM (1971) J Phys Chem 75:1881
4. Kose A, Ozaki M, Takano K, Kobayashi Y, Hachisu S (1973) J Colloid Interface Sci 44:330
5. Crandall RS, Williams R (1977) Science 198:293
6. Mitaku S, Otsuki T, Okano K (1978) Jpn J Appl Phys 17:305
7. Clark NA, Hurd AJ, Ackerson BJ (1979) Nature 281:57
8. Lindsay HM, Chaikin PM (1982) J Chem Phys 76:3774
9. Pieranski P (1983) Contemp Phys 24:25
10. Pusey PN, van Megen W (1986) Nature 320:340
11. Okubo T (1988) Acc Chem Res 21:281
12. Ottewill RH (1989) Langmuir 5:4
13. Okubo T (1993) Prog Colloid Polym Sci 18:481
14. Okubo T (1987) Angew Chem Int Ed Engl 26:765
15. Okubo T, Aotani S (1988) Naturwissenschaften 75:145
16. Okubo T, Aotani S (1988) Colloid Polym Sci 266:1049
17. Okubo T (1990) Colloid Polymer Sci 268:1159
18. Hachisu S, Yoshimura S (1980) Nature 283:188
19. Yoshimura S, Hachisu S (1983) Prog Colloid Polym Sci 68:59
20. Yoshimura S, Hachisu S (1985) J Phys (Paris) 46(C3):115
21. Hachisu S (1990) Phase Transition 21:243
22. Okubo T (1987) J Chem Phys 87:5528
23. Shih WY, Smith WH, Aksay IA (1989) J Chem Phys 90:4506
24. Okubo T (1990) J Chem Phys 93:8276
25. Murray MJ, Sanders JV (1980) Phil Mag A42:721
26. Hachisu S, Kose A, Kobayashi Y, Takano K (1976) J Colloid Interface Sci 55:499
27. Bartlet P, Ottewill RH, Pusey PN (1990) J Chem Phys 93:1299
28. Bartlet P, Ottewill RH, Pusey PN (1992) Phys Rev Lett 68:3801
29. Lindsay HM, Chaikin PM (1982) J Chem Phys 76:3774
30. Pusey PN, van Megen W (1987) Phys Rev Lett 59:2083
31. Baker JA, Henderson D (1967) J Chem Phys 47:2856
32. Wadachi M, Toda M (1972) J Phys Soc Jap 32:1147
33. Hachisu S, Kobayashi Y, Kose A (1973) J Colloid Interface Sci 42:342
34. Brenner SL (1976) J Phys Chem 80:1473
35. Takano K, Hachisu S (1977) J Chem Phys 67:2604
36. Okubo T (1992) Naturwissenschaften 79:317
37. Okubo T (1993) Colloid Polym Sci 96:61
38. Okubo T (1994) Langmuir 10:1695
39. Okubo T (1994) Langmuir 10:3529
40. Okubo T (1987) Ber Bunsenges Phys Chem 91:1064
41. Alexander S, Chaikin PM, Grant P, Morales GJ, Pincus P, Hone D (1984) J Chem Phys 80:5776
42. Okubo T (1988) J Colloid Interface Sci 125:380
43. Okubo T (1990) Colloid Polym Sci 268:1159
44. Okubo T (1989) J Chem Phys 90:2408